NIST Technical Note
NIST TN 2336

Pyrrhotite Reference Material Synthesis

Michael J. Mengason
Stephanie Watson

This publication is available free of charge from:
https://doi.org/10.6028/NIST.TN.2336

NIST NATIONAL INSTITUTE OF STANDARDS AND TECHNOLOGY
U.S. DEPARTMENT OF COMMERCE

NIST Technical Note
NIST TN 2336

Pyrrhotite Reference Material Synthesis

Michael J. Mengason
Stephanie Watson
Materials and Structural Systems Division
Engineering Laboratory

This publication is available free of charge from:
https://doi.org/10.6028/NIST.TN.2336

April 2025

U.S. Department of Commerce
Howard Lutnick, Secretary

National Institute of Standards and Technology
Craig Burkhardt, Acting Under Secretary of Commerce for Standards and Technology and Acting NIST Director

NIST TN 2336
April 2025

Publication History
Approved by the NIST Editorial Review Board on 2025-04-03

How to Cite this NIST Technical Series Publication
Mengason MJ, Watson S (2025) Pyrrhotite Reference Material Synthesis. (National Institute of Standards and Technology, Gaithersburg, MD), NIST Technical Note (TN) NIST TN 2336. https://doi.org/10.6028/NIST.TN.2336

Author ORCID iDs
Michael J. Mengason: 0000-0002-9779-5852
Stephanie Watson: 0009-0003-2001-5592

Contact Information
Michael.Mengason@nist.gov

Abstract

The mineral pyrrhotite was synthesized from iron and sulfur starting materials for one component in a four-component reference material (RM 8154-*Pyrrhotite in Concrete*) to be used to evaluate the presence of sulfur in aggregate (crushed rock) and concrete. Pyrrhotite-bearing aggregate used in concrete has and continues to result in the degradation and failure of residential foundations around Tolland County, CT (Northeastern Connecticut and South-Central Massachusetts). A total of 254 bottles containing 5 grams of synthesized pyrrhotite were produced. This *Pyrrhotite in Concrete* suite reference material will fill a current void in available testing materials and will allow laboratories to advance and unify methods of analysis. Scaling up production of the pyrrhotite component revealed considerations in design and safety that were ultimately incorporated into NIST's synthesis protocols.

Keywords

Pyrrhotite, Synthesis, Aggregate, Concrete, Tolland, Becker's Quarry

Table of Contents

List of Tables

List of Figures

1. Introduction

Degradation of residential concrete foundations to imminent failure has become a significant hardship for homeowners in Tolland County, Connecticut (CT) and surrounding areas [1–7]. Owners of affected homes experience accelerated pervasive cracking of their foundations [Fig. 1] with an associated loss in strength and durability. Concrete is a mixture of cement, sand, water, and aggregate (e.g., small rocks previously mined from naturally occurring deposits but now provided by quarried and crushed rock). Homes were built using concrete that originated from the JJ Mottes Concrete Company in Stafford Springs, Connecticut, including aggregate from Beckers Quarry, Willington, Connecticut, starting in 1983 and continuing for over 30 years [2]. As early as 1993, cracking was identified by the owners of a home built in 1985 on Old Kent Road in Tolland County. Pyrrhotite was not initially reported as a potential cause. In 2008, a petrographer reported pyrrhotite present in samples from a house foundation and identified pyrrhotite oxidation as key to the degradation. Subsequent analysis of hundreds of foundations by several different independent entities has confirmed these findings [4, 5].

Fig. 1 Map cracking in a residential foundation sampled during a NIST field study. Images of a residential foundation slated for removal and replacement showing extensive intersecting fractures termed "map cracking." [Photo Credit: NIST]

The use of aggregate from Becker's quarry was suspended following an agreement with the state government [8] but it was used to build foundations as recently as 2014. Reports of prematurely deteriorating foundations became widespread and began to be investigated, with 550 cases of foundation degradation received by the Connecticut Department of Consumer Protection (CDCP) by 2017 [2]. Typically, pyrrhotite-affected foundations require the expensive remedy of lifting the house from its supporting structure to allow the removal and recasting of the entire basement structure, which can range in cost from

$150,000 to $250,000. The value of the structure is reduced to $0 following the identification of pyrrhotite, preventing its use as collateral for repair loans and reducing the tax income to the town and its ability to provide aid [1]. The Connecticut Foundation Solutions Indemnity Company was set up by the State of Connecticut to provide financial assistance to homeowners. As of October 2024, one thousand families have received aid. [9]. Although most of the affected structures were residential, the Birch Grove School required reconstruction in 2019, broadening the scope of potentially afflicted structures requiring testing.

State legislatures in Connecticut and Massachusetts (MA) have acted to prevent aggregate containing pyrrhotite from being used in residential foundations by requiring quarries to periodically test their aggregate to determine the total sulfur content [10][11]. Aggregate may include sulfide minerals such as pyrite (FeS_2) and sulfate minerals such as gypsum ($CaSO_4 \cdot 2H_2O$) that are not of concern in this instance but contribute to the total sulfur content. This is reflected in the limits adopted [Fig. 2]. Aggregate containing less than 0.1 weight percent (wt. %) by weight total sulfur can be used. Aggregate containing 0.1 wt. % to 1 % wt. total sulfur in samples with no pyrrhotite detected can be used. Aggregate containing 0.1 wt. % to 1 wt. % total sulfur in samples containing pyrrhotite cannot be used. Aggregate containing greater than 1 wt. % total sulfur cannot be used.

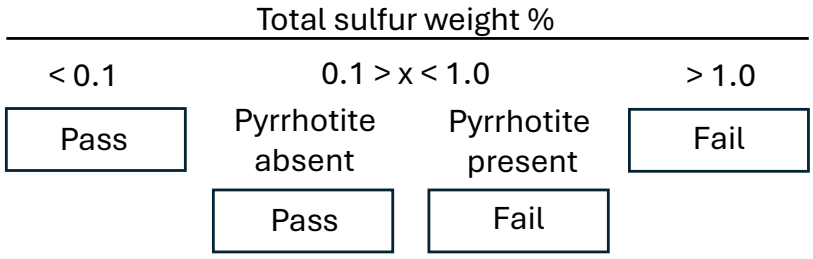

Fig. 2 Currently enacted limits for the full usability of aggregate in concrete based on total sulfur content in weight percent and the presence or absence of pyrrhotite.

To support the development of analytical techniques used to make this determination, and to support the development of standards and methods to ensure consistent interlaboratory results, the National Institute of Standards and Technology (NIST) proposed and has developed a reference material (RM-8154). This Technical Note describes efforts to synthesize the mineral pyrrhotite as one component of this reference material.

1.1. Pyrrhotite Description

Pyrrhotite is a naturally occurring iron-sulfide mineral most frequently described as an accessory mineral identified in small percentages of the total minerals in a range of sedimentary, metamorphic, and igneous rocks. Pyrrhotite present from the formation or alternation of the rock can be further overprinted by the actions of hydrothermal fluids. These hydrothermal fluids are, in some instances, responsible for the deposition of sulfides to the extent that the majority of the rock is composed of sulfides and, along with massive sulfide formations such as Sudbury and other ore-generating environments,

represent a significant source of certain metals (e.g., Cu, Ni, Ag, Au, Pt) [12] This association with metals of economic interest has resulted in considerable research on pyrrhotite and related sulfides.

Pyrrhotite has a non-stoichiometric composition that can be expressed as $Fe_{1-x}S$, where x denotes the presence of vacancies in the structure which may vary from 0 to 0.125 depending on polytype. These vacancies allow for the presence of both Fe^{2+} and Fe^{3+} in proportions depending on the fugacity (chemical potential with consideration of pressure) of sulfur in the system [13]. At high temperatures, a range of compositions is stable as a complete solid solution between the most iron-rich and iron-poor members [14]. At the conditions that prevail at the earth's surface, five discrete compositions of pyrrhotite are stable, denoted 4C (Fe_7S_8) which is ferrimagnetic and has a monoclinic structure and a unit cell four times larger in the C axis direction, and 5C (Fe_8S_9), 6C ($Fe_{11}S_{12}$), 7C (Fe_9S_{10}) and 11C ($Fe_{10}S_{11}$) which are not magnetic and may be monoclinic or hexagonal. Of these, the 4C type is the most common [15] and is the target of this synthesis.

Pyrrhotite of the monoclinic type synthesized in this study was first identified by Bystrom in 1945 [16] in a study of natural samples heated in evacuated sealed silica tubes. Bertaut, in 1952 [17], confirmed pyrrhotite of composition Fe_7S_8 is monoclinic. Gronvold and Haraldesn, in 1952 [18], synthesized monoclinic pyrrhotite at 290 °C from elemental starting materials in evacuated silicate tubes using a method like the current study. Many researchers over succeeding decades have utilized the evacuated silica tube method to generate small amounts of pyrrhotite, generally on the order of grams [19–24]. A primary goal of this report is to describe adaptations of the silicate tube method used in the current program to aid production and safety.

1.2. Disequilibrium

Prior to the mid-1900s, aggregate was generally dug and sieved from natural deposits of rock that had been broken down and transported by natural weathering and erosional processes. These processes allowed for the minerals in the rock to largely equilibrate with the oxidizing environment of our atmosphere following removal from the generally reducing oxygen-poor environment of bedrock. Quarried and crushed rock, in comparison, has no such opportunity to equilibrate before emplacement in concrete. The results of this sudden exposure to water and oxygen on sulfide minerals can be seen in the waste runoff from many mines and mine tailings piles where sulfuric acid produced by the oxidation of sulfide minerals damages local ecologies [25–27]. A study comparing 235 aggregate samples from quarried sources and natural deposits in Norway identified 22 samples that contained greater than 0.1 wt. % sulfur, with 19 samples containing pyrrhotite greater than 0.14 wt. % sulfur (local acceptable limit), all from quarried aggregate. None of the natural deposits contained greater than > 0.1 weight percent sulfur [28]. The wide availability of natural aggregate (granitic and granodioritic) sieved from Eskers (sub-glacial deposits) in Finland was credited with the low instances of pyrrhotite oxidation in concrete in a survey of concrete damage [29]. Globally, however, the broad depletion of natural formations and

improvements in rock-crushing methods have resulted in a transition to quarried and crushed rock, increasing the potential for pyrrhotite-related concrete degradation.

1.3. Widespread Occurrence

Concrete degradation due to pyrrhotite oxidation is neither a new nor localized occurrence. Pyrrhotite is a common accessory (i.e., small weight fraction) mineral in metamorphic and igneous rocks and can be found in some sedimentary rocks. Consequently, rocks containing pyrrhotite are widespread, and other cases of pyrrhotite-induced degradation have been reported in North America and Europe and can reasonably be expected to occur worldwide. In Oslo, Norway, concrete degradation was linked to pyrrhotite, which was investigated in 1959 [30]. Concrete in contact with shale (from the sedimentary Alum Shale formation) was affected by sulfate attack through the groundwater, while concrete incorporating the shale as aggregate demonstrated cracking with the deposition of iron-oxide phases. In Switzerland, concrete in a dam showed expansion beginning in the 1980s and damage due to pyrrhotite oxidation was studied in 2011 [31] In the Spanish Pyrenees, dams at Tórán, Graus, and Tavascan had documented map cracking determined to be from pyrrhotite in aggregate schist (metamorphic rock) starting in 1995 [32–34]. Black shales (sedimentary rock) containing pyrrhotite from a quarry near Madrid were studied for reactivity after buildings demonstrated cracking in the 1970s [35]. Miocene marlstone, a Cretaceous limestone, and an Ordovician shale (sedimentary rocks) from Northern Spain, known to contain pyrrhotite, were studied for reactivity [36]. In the Trois-Riviéres area in Quebec, Canada, pyrrhotite in anorthositic gabbro (igneous rock) aggregate was identified in 2005 as a cause of widespread damage to foundations [5, 37, 38]. The gabbro contains a complex sulfide assemblage, including pyrrhotite, pyrite (FeS_2), chalcopyrite ($CuFeS_2$), and pentlandite (approximately $(NiFe)_9S_8$). In County Donegal, Ireland, pyrrhotite in a phyllite (metamorphic rock) aggregate incorporated into cast concrete blocks used in the walls of homes has resulted in cracking requiring replacement, with evidence accumulating since 2017 [39–42]. Degradation due to pyrrhotite oxidation is clearly not limited to any one rock type. It is possible that some types may allow oxygen and water ingress to the pyrrhotite more rapidly, and some types may fracture more easily, allowing further ingress. But in each case listed, the result was fundamentally the same. In this context, the problems in Connecticut and Massachusetts are unfortunate examples of a repeating “newly identified” problem that is only now being prevented with regulations to prohibit the use of pyrrhotite-containing aggregate in construction.

1.4. Connecticut and Massachusetts Geologic Context

The current reference point for the distribution of rock types in Connecticut is the geologic map of Rogers 1985 [43]. Becker’s quarry lies in the Brimfield Schist, part of the Merrimack Synclinorium in the Eastern Uplands of Connecticut. The state can be broadly divided into the Western Uplands, the Central Lowlands, and the Eastern Uplands [44]. The surface of Connecticut today is a horizontal slice through a once much larger Appalachian Mountain

range formed by the sequential collisions of a proto-North American continent (Laurentia) and a microcontinent (Avalon) followed by the continent of Africa, which completed the closure of the Iapetus Ocean and the formation of the North American portion of Pangea. In the orientation of North America today, the landmasses would appear to have approached from the northwest and southeast, resulting in thin elongated rock units that trend northeasterly into Massachusetts. The parent material of the rocks of the Brimfield and related Tantic Hill formations formed in the shallow sea that temporarily existed between Laurentia and Avalon. Thick layers of sediments varying in composition with distance from the landmasses were formed. With the closure of the ocean, the sediments underwent increasing burial that imposed elevated pressure and temperature. Later alteration by the actions of hydrothermal fluid flow overprinted the variation in chemistry inherent in the source [45]. Now exposed at the surface, these formations show variations in metamorphic grade and mineralogy across the mapped units [46].

The Brimfield Schist contains interlayered biotite schist and gneiss with minor areas of amphibolite and calc-silicate rock. Accessory minerals representing small mass fractions include tourmaline, magnetite-ilmenite, pyrite, monazite, zircon, apatite, rutile, and graphite [47]. Beckers Quarry overlays an altered hydrothermal vein which produces extensive but heterogenous pyrrhotite deposition. Most aggregate samples from the quarry that contain pyrrhotite do not contain pyrite, in contrast to samples from the Trois Rivier area. Some sampled aggregate from Beckers quarry has shown pyrite in conjunction with graphite and rutile but this is not the usual occurrence. Pyrite is generally much less reactive than pyrrhotite, except for framboidal pyrite [48], which is not the type described here. The pyrrhotite within aggregate is most often present in thin flame-like ribbons among biotite or muscovite layers. The amount of pyrrhotite is highly variable among aggregates ranging from no sulfides to some that are largely composed of pyrrhotite that likely grew in veins. As a result, the percent of sulfur due to pyrrhotite in concrete incorporating aggregate from Beckers quarry will vary significantly within a structure, and testing must be sufficient to represent the structure.

1.5. Pyrrhotite reactions

As previously stated, pyrrhotite undergoes oxidation upon contact with air and water. This results in a cascading series of reactions replacing the cementing (bonding) minerals in the structure with ones of greater volume, generating expansive forces within the structure [25, 36, 49–54]. Ultimately, this conversion of the existing mineral structure of the cement paste combined with the generated expansive forces yields extensive connected fracture networks, which significantly reduce the strength and cohesiveness of the structure [38, 55]. The reactions involved can be considered in two stages. The equations presented here are simplified examples of likely scenarios.

In the initial stage, oxygen and water gain access through fractures and possibly within biotite [56] and react with pyrrhotite to produce an iron-oxyhydroxide as well as sulfate and hydrogen ions [34]. [Equation 1]

$$Fe_7S_8 + 17\tfrac{1}{4}O_2 + 11\tfrac{1}{2}H_2O \Longrightarrow 7FeO(OH) + 8SO_4^{2-} + 16H^+ \quad (1)$$

As written, the oxyhydroxide might be goethite or lepidocrocite. Ferrihydrite, a nano-crystalline phase, has been suggested as a potential reaction product with a greater volumetric increase [34]. Ferrihydrite is commonly found in soils associated with geothite. Multiple compositions are reported for the mineral ferrihydrite in the literature [57]. The formula $Fe_{10}O_{14}(OH)_2$ is commonly used; however, the nature of water inclusion in ferrihydrite is complex. Ferrihydrite has been represented by the formula $Fe(OH)_3$ in some sources but would correspond to the mineral bernalite. Any of the oxyhydroxide phases formed are deposited in the space previously occupied by pyrrhotite as well as in fracture spaces within pyrrhotite and fractures elsewhere in aggregate [Fig. 3]. The volume of these is greater than the pyrrhotite they replace providing an expansive pressure within the aggregate. This could logically expand fractures opening the pyrrhotite to further oxidation.

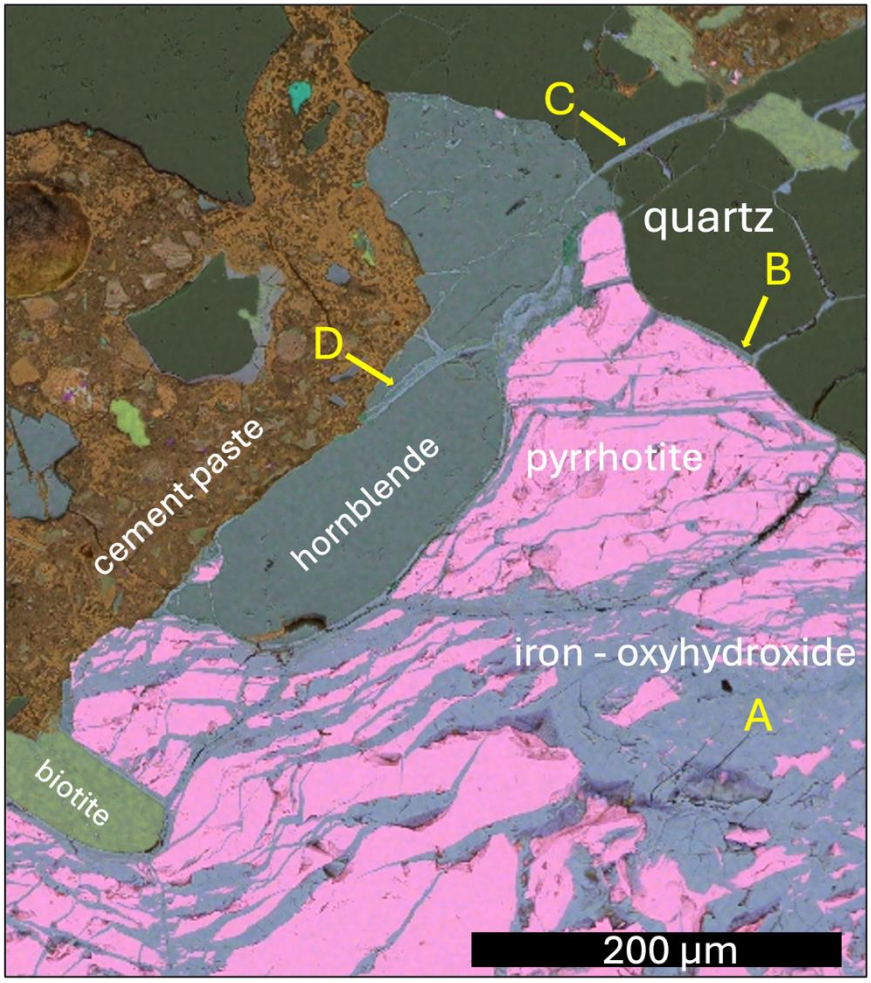

Fig. 3 Iron-oxyhydroxide oxidation products in SEM. Composite false-color image with element maps by energy dispersive spectroscopy (EDS) overlaid on a backscatter (BSE) micrograph of a cut and polished sample of concrete from the foundation of the Birch Grove School in Connecticut. Pyrrhotite (pink) oxidation results in iron oxyhydroxide (light blue/gray) reaction products as a replacement (A) at the edge of pyrrhotite (B) as well as filling fractures in quartz (C) and hornblende (D).

In the second stage, sulfate and hydrogen ions travel to the cement paste and react with components there. Formulas written here are presented in cement chemist notation: C = CaO, $\overline{C}$=CO_2, S=SiO_2, $\overline{S}$ = SO_3, A =Al_2O_3, H = H_2O. Within the first few years of cement hydration, the clinker phase aluminate (C_3A) may react with the cement phase portlandite (CH) incorporating sulfate and water and producing monosulfate ($C_4A\overline{S}H_{12}$, an afm phase, Equation 2) or ettringite ($C_6A\overline{S}_3H_{32}$, an aft phase, Equation 3). These reactions consume a matrix phase of the cement potentially disturbing the structure of the paste and producing a phase significantly larger, providing additional expansive pressure within the matrix.

$$CH + C_3A + \overline{S} + 11H \Longrightarrow C_4A\overline{S}H_{12} \quad (2)$$

$$3CH + C_3A + 3\overline{S} + 29H \Longrightarrow C_6A\overline{S}_3H_{32} \quad (3)$$

Gypsum ($C\overline{S}H_2$) may form from portlandite at any age [Equation 4].

$$CH + \overline{S} + 2H^+ \Longrightarrow C\overline{S}H_2 \quad (4)$$

In older concrete, the available aluminate will have been largely consumed and be unavailable for reaction. Monosulfate can provide a source of aluminum for ettringite formation in this case (Equation 5).

$$C_4A\overline{S}H_{12} + 2C\overline{S}H_2 + 16H \Longrightarrow C_6A\overline{S}_3H_{32} \quad (5)$$

At low temperatures (<8°C), the mineral thaumasite ($C_3S\overline{CS}H_{15}$), may form [37][58][59][60][61][62]. Thaumasite formation requires carbonate from carbon dioxide or limestone included in the concrete. Calcium silicate hydrate gel (C-S-H, simplified as $C_3S_2H_3$ here) in the cement paste can react with either portlandite (equation 6) or by conversion of ettringite (equation 7). In the latter case, aluminum may be made available for further sulfate formation. The primary bonding phase of the cement paste (C-S-H) is therefore consumed in these reactions, and its products simultaneously exert expansive pressure within the matrix.

$$C_3S_2H_3 + 3CH + 2\overline{S} + 2\overline{C} + 11H \Longrightarrow 2C_3S\overline{CS}H_{15} \quad (6)$$

$$C_3S_2H_3 + C_6A\overline{S}_3H_{32} + 2\overline{C} + 2\overline{S} + H \Longrightarrow 2C_3S\overline{CS}H_{15} + 3C\overline{S}H_2 + A \quad (7)$$

Specific temperature and chemical conditions within the concrete will ultimately determine the reactions that take place, and those reactions may change over time. However, the net result of all the reaction pathways is a degradation of the cement paste and expansion.

1.6. Measuring Sulfur Content

Several methods have been adopted to measuring sulfur in concrete to evaluate existing structures as well as in aggregate to allow screening for several reactive minerals, including pyrrhotite, prior to potential use. As stated previously, a tiered limit structure for sulfur content has been adopted by Connecticut and Massachusetts [10][11]. Methods of analysis capable of high accuracy and precision at these low concentrations are therefore required.

The most commonly used methods to evaluate the sulfur content of a powdered bulk sample involve the use of a carbon/sulfur element analyzer [63] or an X-ray fluorescence spectrometer (either energy dispersive-ED-XRF or wavelength dispersive-WD-XRF) [51, 64–70]. Carbon/sulfur elemental analyzers use combustion in a thermally or inductively heated vessel in an oxygen stream. The resulting SO_2 gas is then passed through an infrared detector and quantified. This method requires the sample to be ground to a specific particle size to optimize complete sample consumption but may be used only to determine total sulfur and has been shown to be sensitive to specific laboratory practices of sample preparation and combustion methods. X-ray fluorescence spectrometry (either ED-XRF or WD-XRF) can be used to determine the total sulfur content of samples of either aggregate or concrete prepared as either a packed powder pellet or as a fused disk, depending on the method. Analysis of packed powder samples by WD-XRF can further evaluate the ratio of sulfide to sulfate in the sample [68, 70] allowing an analyst to separate the total sulfur content into the contribution from sulfates and the contribution from sulfides. XRF is a standards-based method that is sensitive to differences between the matrix and the physical preparation (e.g., particle size, packing) of the sample and the standard.

Reference material RM 8154, for which pyrrhotite is being synthesized, is designed to allow analysts to mix reference materials to match the sample matrix and the needed sulfur content range of their unknowns, regardless of the method utilized. It can help to evaluate method precision and compare results across instruments and among laboratories.

Other bulk analytical techniques may potentially be used to measure sulfur concentration, particularly given the CT and MA state pyrrhotite concentration requirements for aggregate used in concrete materials. X-ray diffraction (XRD) is widely used to analyze aggregate and concrete [71]; however, the acceptable sulfur concentration for an aggregate is below its limit of quantitation of 2 wt. % – 5 wt. % constraining its utility [67, 72]. Traditional wet-chemical methods are an option but are not as commonly used today [73][74]. An acid-leaching procedure was proposed by Marcelino et al., which could separate the proportion of total sulfur due to pyrrhotite from that due to pyrite, which would remain after treatment [75][76]. Guiruis describes a method utilizing mass-loss following sample immersion in oxidizing fluid [77]. A drop in the magnetic susceptibility of pyrrhotite between 310 °C and 325 °C has been used to measure pyrrhotite in a heated sample [78].

Aggregate and concrete are also examined with in-situ techniques capable of studying the identity of minerals and their microstructural relationships on small scales. The 0.1 wt. % /

1 wt. % limit for total sulfur requires identifying if pyrrhotite is present. The following methods are used for this purpose and to investigate evidence of pyrrhotite oxidation in concrete.

Optical petrography has a long history of use with rock and concrete samples [79][80][81] that have been prepared as polished thin sections on glass slides. Concrete is routinely examined by optical petrography to identify problems such as Alkali-Silica reactions (ASR), Alkali-Carbonate reactions (ACR), excessive water-to-cement ratio in the cement mix, and insufficient sand or aggregate. Pyrrhotite is an opaque phase and cannot be identified by the transmission polarized light microscopy (PLM) used to examine prepared thin sections. However, reflected light PLM, which many petrographic microscopes can use, can discriminate among the sulfide phases, allowing it to be used as an accessory method to one of the bulk methods described above [69].

Samples prepared either as polished slices of rock or concrete or as thin sections can be investigated using Scanning Electron Microscopy (SEM) [82][83][84][85]. Samples for SEM require a very high level of polish and are generally coated in a thin layer of carbon or metal. This allows the examination of smaller features than optical microscopy. It is often used in addition to optical petrography but may be used alone. Electron microscopy with energy dispersive spectrometry (EDS) can determine the chemical composition of phases and identify pyrrhotite. SEM images or images combined with chemical maps can be analyzed to determine the fractional area of a given mineral [Fig. 4]. SEM/EDS can be coupled to “automated mineralogy” methods to compare either spectra to recorded standards or by comparing compositions to established ranges. This allows larger numbers of points to be analyzed making the analysis more representative. [86][75]

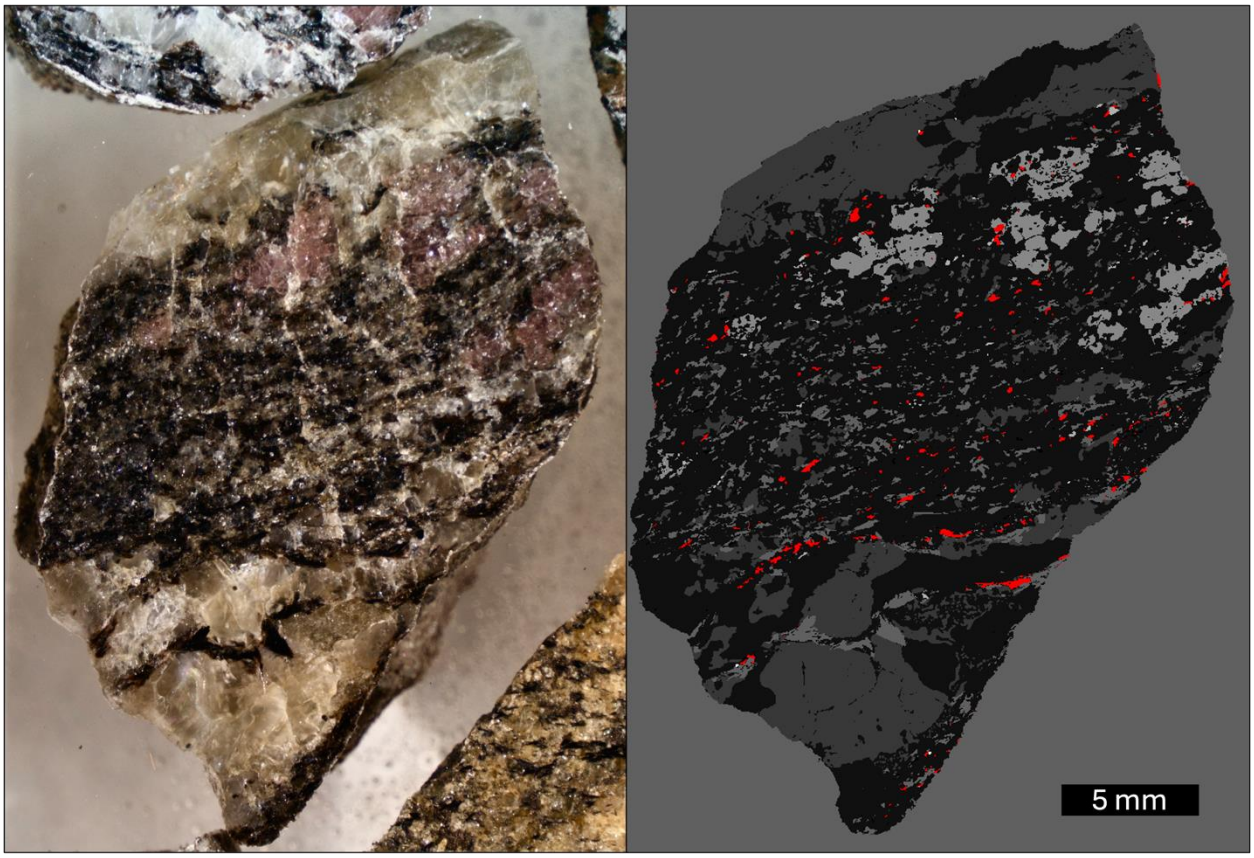

Fig. 4 Segmented image of pyrrhotite in aggregate from Beckers quarry in Connecticut. Binocular microscope image (left) and segmented SEM image made from many image tiles (right). Pyrrhotite (red) is dispersed and follows the layers of the gneissic banding defined by silicate minerals (greys).

Micro-XRF (μXRF) uses a narrow X-ray beam to analyze a small area of the sample, like the way an SEM uses an electron beam, and can similarly be used to scan a sample for sulfides [87]. Micro-XRF uses energy dispersive detection and similarly can give information on the chemical composition of minerals analyzed. Quantification of the elemental ratios is different than that of SEM and can be challenging. The spot size for μXRF is larger than that for SEM and lacks the resolution to investigate the smallest features, but can be used to qualitatively assess or rank specimens that would require further analysis. Moreover, sample preparation for μXRF is less intensive than for SEM as the surface may not need to be as carefully prepared, including carbon coating and precise polishing.

For samples that have been determined to have a total sulfur content in the 0.1 to 1 wt. % range, Rodrigues et al. 2016 [63] proposed a system to evaluate if the aggregate would be likely to show expansion and cause deleterious effects, similar to that which was used to test for alkali silica reaction potential. He proposed an oxygen consumption test where ground aggregate would be exposed to air and water [88] based on acid mine tailings studies [89][90]. The oxygen content of the air is measured. This is followed by a modified mortar-bar test with aggregate cast in cement and exposed to NaOCl (bleach) to accelerate oxidation [91]. Expansion of the mortar bar is indicative of pyrrhotite reaction

and the unsuitability of the aggregate for use in concrete. An alternate approach for accelerated testing of concrete has been proposed by Ojo et al. 2024 [92] and Araiza et al. 2023 [93] in which a current applied across a concrete sample accelerates the oxidation.

1.7. A Reference Material

With a wide range of techniques and potential variation in procedures among laboratories using the same methods, it is essential to ensure that, in any instance, a given sample would yield the same results regardless of the laboratory conducting a given test. A suitable reference material for sulfur in aggregate and concrete is not available. The National Institute of Standards and Technology (NIST) developed a plan for a multiple-component reference material (RM) that simulates a concrete matrix for laboratories and other stakeholders to use for method development and validation of methods. Reference materials are homogenous for one or more specified property values. These are separate from Standard Reference Material (SRM), which carries a standard reference material certificate (Certificate of Analysis) and has a more lengthy development period and certification process. RM-8154 contains ground samples of quartz sand, hydrated Ordinary Portland Cement (OPC), and a sample of sulfide-bearing gabbro aggregate (Quebec, Canada) to be used with a mix design to generate a series of custom calibration samples best suited for analytical techniques and expected ranges of sulfides. An additional component of powdered pyrrhotite was included to extend the range of achievable sulfur concentrations and allow for standard addition to achieve precise pyrrhotite concentrations to accurately evaluate techniques. Naturally occurring pyrrhotite tends to have non-iron metallic impurities (e.g., Cu, Ni, Zn) and inclusions of other minerals (e.g., pyrite, chalcopyrite, pentlandite, sphalerite) [94]. To provide a source of pyrrhotite with limited impurities, a method of synthesizing the mineral by heating pure iron and sulfur reagents within sealed evacuated fused quartz tubes was selected. This method is generally used to make quantities of a few grams. Developing the techniques to produce the larger quantities (hundreds of grams) required for the reference material revealed several aspects of the equipment and experimental design that needed to be considered and are the focus of this document.

2. Methods

2.1. Overview

The general synthesis process used in this project involved heating iron and sulfur starting reagents sealed in evacuated quartz-glass ampules in a series of temperature steps as shown in Fig. 5. From 150 °C to 250 °C, the reaction would produce pyrite, a mix of pyrrhotite compositions, and unreacted iron. Inspection of the ampule and material indicated liquid sulfur was consumed within 24 hours. At 650 °C the grains homogenize to pyrrhotite solid solution of approximately Fe_7S_8 composition with a hexagonal structure. Twenty-four hours were allotted for this homogenization to ensure completeness. In the final steps, grains were allowed to recrystallize to the monoclinic structure at 250 °C for at least 24 hours; however, many samples remained for 48 hours or more, due to staff schedules. The development of this method progressed as challenges to scaling up were identified and resolved, as will be described.

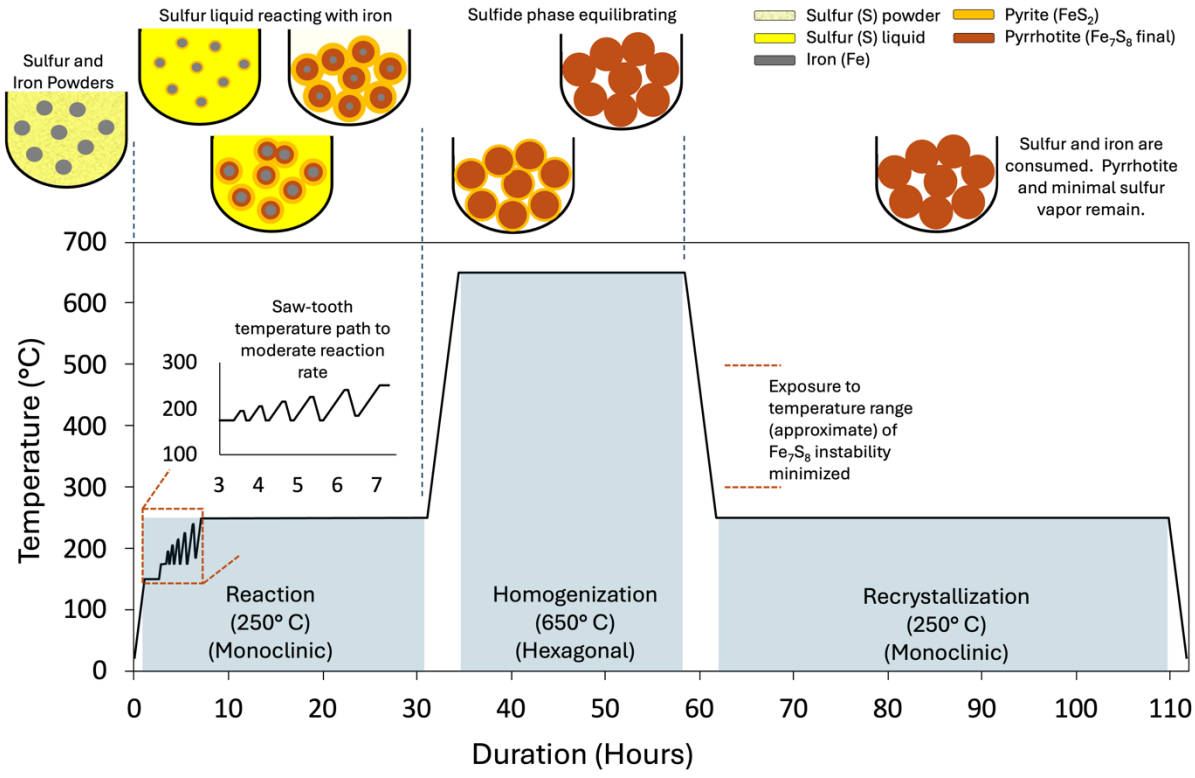

Fig. 5 General synthesis process description. Iron powder mixed with sulfur powder in sealed evacuated silica tubes is allowed to react in a multi-step heating process (top). The temperature profile (bottom) shows an initial reaction period at lower 250 °C following a saw-tooth heating pattern, a homogenization period at 650 °C, and finally, a period at 250 °C to promote recrystallization from the high-temperature hexagonal form of pyrrhotite to the low-temperature monoclinic form.

While initial trials did not suffer any loss of individual ampules due to breakage, a test of 5 ampules concurrently failed due to overpressure, resulting in their loss. The results of overpressure resulted in minor damage to equipment, which was contained within the

furnace by its structure. This prompted a reexamination of the synthesis process, and several changes were made based on suspected causes such that these failures were eliminated. This included reducing the reagent mass, increasing the free volume in the ampule, changes to the construction and assembly of the ampule, and modifying the temperature profile. However, some ampules were found to have cracked, and the contents oxidized during some experiments. These 'quiet failures' have been reduced through continued improvements in the glassware of the ampule but persist.

2.2. Materials

2.2.1. Reagents

Reagent powders were purchased from Thermo Fisher Scientific. "Iron Powder, spherical 99.9 %" was purchased in 250 g quantities. Initial shipments had a grain size of < 10 µm. Later shipments had a grain size of < 20 µm. "Sulfur powder sublimed 99.5 %" was sized as 100 mesh. Initial trials used 70 g of starting mixture of 60.4 % Fe and 39.6 % S by mass. Later experiments used 40 g, 45 g, or 50 g. Powders were gently stirred with a glass rod in a glass beaker to mix. Iron and sulfur powder should never be ground together in a mortar and pestle to prevent fire hazards.

2.2.2. Ampules

Fused quartz tubing was purchased from TGP (Technical Glass Products Company, Painesville, Ohio). Quartz tubes were ordered in several batches from the manufacturer. Ampules had 2 mm wall thickness (WT) with 15 mm Interior Diameter (ID). Some early experiments developing the method were performed with 2 mm WT and 16 mm ID. Initial ampules were fabricated at NIST in the glass shop as needed by sealing and rounding one end of a section of tubing and then thinning or "necking down" a section using an oxygen methane flame. Later, ampules were fabricated by the company Strong Force Glass in batches by sealing and rounding one end of a 250 mm section of tubing and reducing the diameter of the other with a 9.5 mm radius of curvature for fusing with a section of 2 mm WT / 4 mm ID tubing (100 mm long). This provided a more consistent supply of ampules. Ampules were filled with reagents and evacuated to a pressure (vacuum) below 1×10^{-2} Pa. The narrow "neck" only of the ampule was heated with a narrow oxygen/methane flame to allow the glass sides to pull closed under vacuum and then heated further to melting at that point and separated ("tipped off"). Glassblowers noted hairline flaws in the fused quartz glass tubes arriving from the manufacturer (Technical Glass Products) that were visible only when heated when they appeared as brighter linear features in the glow from the glass. These flaws inherent in the manufacturing process would reduce the tensile strength of the fused quartz. The tubes were heat-treated end-to-end with the torch before ampule fabrication to allow the glass to seal itself. Ampules were wrapped in quartz-fiber tubing and a net of stainless-steel wire to provide containment in the event of an

overpressure failure. Ampules at several stages in the process of preparation are presented in Fig. 6.

Fig. 6 Ampules at different stages of preparation. Top to bottom: empty ampule, with filling funnel, with adaptor for vacuum system including silica wool filter, sealed ampule (white at the top of the glass is additional silica wool filter in ampule stem), ampule in silica fiber and stainless-steel wrapping.

2.3. Ampule Design Considerations

The ampule's dimensions were determined after considering the benefits and drawbacks of different options. Ampule size was created to be as large as could fit in the furnace (usable area 160 mm tall, 290 mm wide, 340 mm deep) to facilitate the production over several experiments of a sizeable total quantity of pyrrhotite (1.8 kg) while ensuring the ampule would not overpressurize. It was recommended by a NIST glassblower that a wall thickness greater than 2 mm would make the “tipping-off” process (e.g., when the narrow section of the tube is heated in an oxygen-methane flame and closed under the pull of the vacuum) would have required more extensive heating of that area, the degree of which can be difficult to control. Using a 2 mm thickness as a starting point, the expected pressure of the sulfur volatile phase was considered to help determine the diameter of the tubing. At 650 °C, the sulfur volatile pressure in equilibrium with sulfur liquid is calculated to be

approximately 1000 kPa based on data from NIST/TRC Web Thermo Tables [95]. Working pressure in a quartz-glass tube is related to the hoop stress by equation 8, where S = hoop stress (Pa), p = working pressure (Pa), r = inside radius of the tube (mm), and t = wall thickness (mm).

$$S = \frac{pr}{t} \tag{8}$$

The recommended design limit for quartz glass uses a maximum tensile strength of 7×10^6 Pa. This is less than the ideal tensile strength and includes a factor of 7 reduction to account for imperfections, particularly on the glass surface. In Fig. 7, calculated sulfur vapor pressure for sulfur liquid [95] and pyrite [96] is plotted against temperature. The 15 mm ID tubing provides a significant margin for error based on the maximum temperature of 650 °C used here. However, as the sulfur liquid would ideally be consumed at the lower pressures encountered at 150 °C to 250 °C, the pressures at 650 °C would more closely reflect the curve shown for sulfur vapor in equilibrium with pyrite.

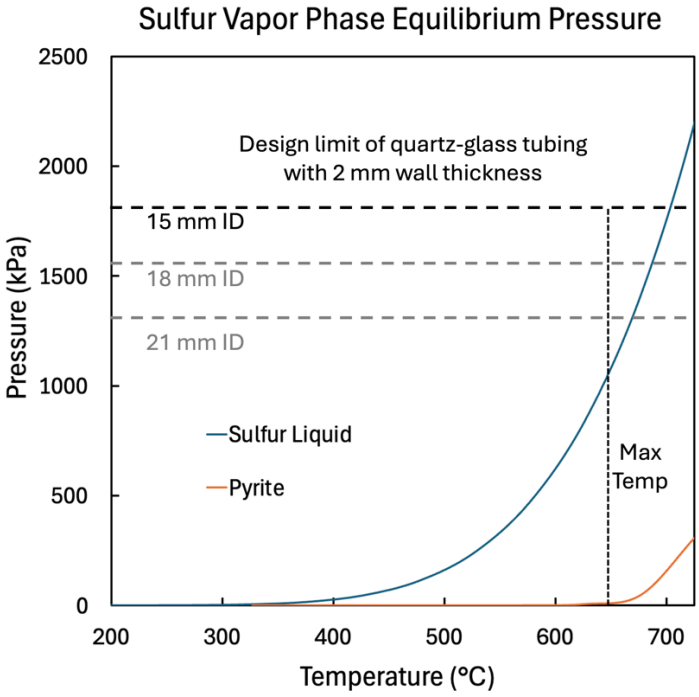

Fig. 7 Calculated pressure of the sulfur vapor phase in equilibrium with liquid sulfur (blue [95]**) and pyrite (orange** [96] **as a function of temperature. At the maximum temperature of experiments the expected pressure is well below the design limit of 15 mm ID, 2 mm WT tubing used.**

2.4. Temperature Path Considerations

Data on the expected phase stability in the Fe-S system are shown in Fig. 8. During the reaction phase (1) and during the recrystallization phase (3), the bulk starting composition is stable as monoclinic pyrrhotite Fe_7S_8 (4C). From approximately 275 °C to 500 °C (a range of exact temperatures are reported by different authors), the bulk composition would be

stable as a more iron-rich composition of pyrrhotite (solid solution) and pyrite. Time in this field is minimized on heating and cooling. Pyrrhotite with a hexagonal structure of the composition Fe_7S_8 is stable as the sample is held at 650 °C, allowing the grains to homogenize (2).

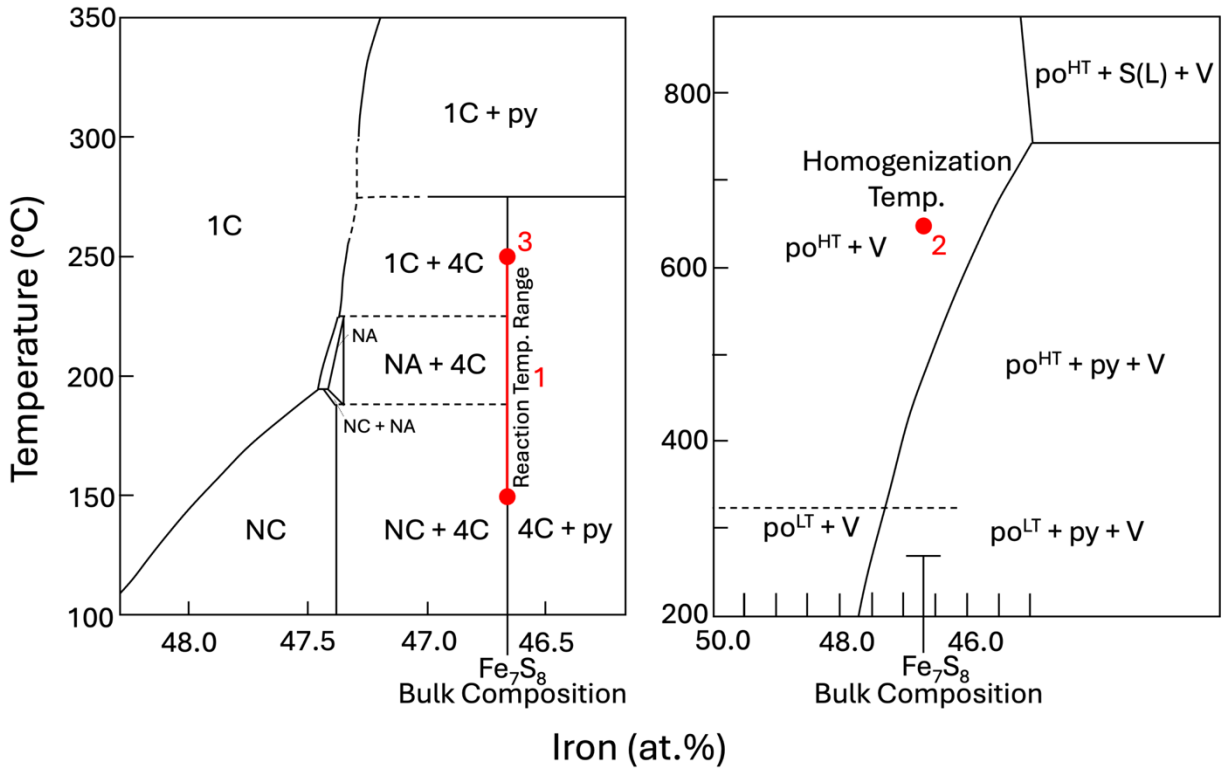

Fig. 8 Phase diagrams for the Fe-S system. (Left) Figure from Sugaki (1977) [96]. Bulk composition is stable as monoclinic Fe_7S_8 (4C) during the reaction stage (1) of the synthesis and in the final recrystallization stage (3) (250 °C). (Right) Figure modified from Toulmin and Barton (1964) [20]. Bulk composition is stable as hexagonal (HT, high temperature) Fe_7S_8 at the homogenization temperature (650 °C) (2). The heating/cooling path minimizes the time between ~300 °C to 500 °C where it is unstable.

2.5. Exothermic reaction considerations

The reaction here between iron and sulfur is exothermic. The enthalpy of formation at temperatures of interest from sulfur and iron for FeS in the liquid phase is -68.81 kJ/mol, and the solid phase is -101.67 kJ/mol. Likewise, FeS_2 as pyrite is -167.36 kJ/mol, and marcasite is -171.54 kJ/mol [35]. As a result, the reaction provides a source of heat and can raise the temperature inside the ampule above the temperature of the furnace. This would increase the pressure of the sulfur volatile phase and the likelihood of an overpressure in the vessel. In Fig. 9, the temperature of the ampule, measured by a thermocouple within the silica sheath, is plotted with a thermocouple located next to the ampule in the furnace. In the figure, the internal temperature of the ample exceeded the furnace temperature by 65 °C for a short period, likely indicating that in a small volume of

the reagents, the reaction was accelerating. The temperature profile in this experiment (plot on left side of Figure 4) was raised from 150 °C to 170 °C and back, then 180 °C and back, etc., allowing reagents to cool after each step. This "saw-tooth" profile allows the reagents to react, but the lack of an external source of heat allows the temperature to subside and avoid overheating. This was the method adopted.

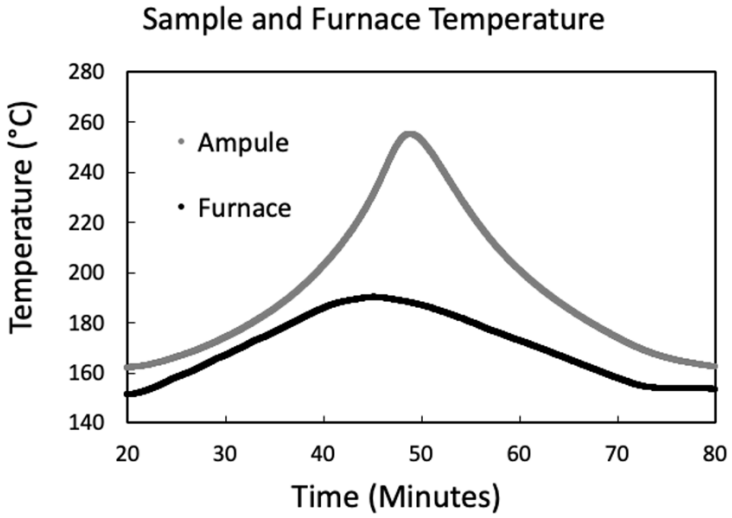

Fig. 9 Recorded temperatures during a synthesis experiment. The light gray line is the temperature at the surface of the ampule recorded by the thermocouple placed within the silica sheath. The black line is the temperature as determined by a thermocouple placed nearby. Heating from the reaction of iron and sulfur led to excess temperature that was allowed to dissipate before the next heating cycle.

2.6. Ampule Filling Considerations

Initial tests of the method used a filling of 70 g in a vessel approximately 250 mm long. This left only approximately 40 mm of unfilled vessel. Initially, this free space was minimized to reduce the amount of sulfur that would end up in the volatile phase and change the bulk composition of the solid. However, it was realized that this effect would be minor, and leaving the ampule less filled could help prevent rupture of the ampule in two ways: 1) an increase in empty volume in the ampule would reduce the intensity of a sudden pressure rise due to evaporating sulfur, and 2) a reduction in the fraction of the cross-section filled with pyrrhotite prevents a potential failure mode given the difference in thermal coefficient between pyrrhotite and the quartz ampule. Quartz-glass is used rather than typical soda-lime glass in these applications due to its higher softening and melting points, less complex chemistry, and low thermal expansion coefficient. Glass can shatter due to variations in temperature throughout the material, including within the thickness of the glass, that lead to expansion or contraction at different rates. In contrast, quartz glass undergoes very little change. In this case, the thermal expansion coefficient of quartz glass is 5.5×10^{-7} cm/cm °C while pyrrhotite is 7.4×10^{-5} cm/cm °C [98]. If the ampule was packed and formed a solid cylinder of pyrrhotite at 250 °C, then on raising the temperature to 650 °C the diameter of the 15 mm diameter pyrrhotite cylinder would expand by approximately 0.44 mm. In contrast, the diameter of the quartz tube would expand by only

0.0014 mm. This would exert outward pressure on the tube and may contribute to a failure. Providing room for expansion reduces this likelihood and so was used in the synthesis procedure.

2.7. Ampule Opening After Completion of Synthesis

Glass ampules have the potential to produce sharp edges upon breaking and represent a cut hazard. To minimize this hazard the following precautions were used: 1) the work was performed in a fume hood with a vertical glass pane between the worker and the ampule, 2) cut-resistant gloves were worn, 3) the ampule was wrapped in fabric to contain any glass shards, and 4) the ampule was pre-cut around half of the circumference to give the break a smooth feature to follow. Ampules were scored with a diamond saw perpendicular to the long dimension to a depth of approximately 0.5 mm to 1 mm. A triangular metal piece was placed in a fume hood on a sizeable clean laboratory tissue. With the cut facing up, the ampule was pressed down firmly and sharply on the triangle repeatedly until it broke [Fig. 10]. In many samples, this resulted in a nearly clean severing of the ampule into two halves. The solid core of pyrrhotite was removed by tapping the ampule on the surface of the fume hood or pulling the core with tweezers. All cores were stored along with any loose pieces of pyrrhotite collected from the chem-wipe in a sample bag.

In some cases, the ampule shattered within the cloth. The cloth wrapping in these cases was opened and laid flat, and pieces of pyrrhotite were removed with tweezers and placed in the collection bag. A magnet was then used to collect the loose pyrrhotite, which ranged in size from a few millimeters down to a dusty coating. The magnet helped to prevent shards of the silica tube from being included with the pyrrhotite. In some samples, the shattering was accompanied by a notable “popping” noise which could represent a difference in pressure (positive or negative) in the ampule compared to ambient pressure. Alternatively, it could have been due to strain in the glass being released.

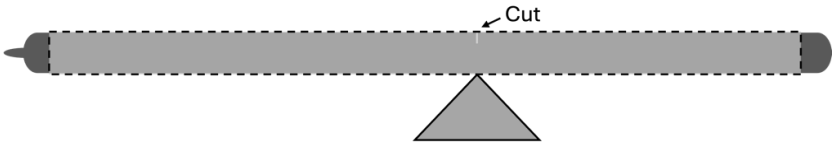

Fig. 10 Setup for ampule opening. The ampule was scored with a thin diamond-bladed saw, wrapped in fabric, and pressed down on a triangular-shaped metal block. Small pieces were collected with a magnet to leave behind shards of the silica.

2.8. Final Reference Material Preparation

Following spot checks on the contents of 6 ampules, the collected pyrrhotite from all ampules was ground in a ring-and-puck mill and sieved to pass through a 200-mesh sieve (63 µm opening size). Samples were stored in a single container under vacuum until bottling. Sample bottles were loaded with 5 grams of the powdered pyrrhotite using a riffle sorter. Samples were bottled under nitrogen and stored in vacuum packs to prevent

oxidation of the contents. This bottling was performed in the NIST Office of Reference Materials.

3. Results

Thirty-seven ampules in total were produced [Fig. 11]. Approximately 1.8 kg of starting materials were converted into sulfide minerals. Six ampules that covered the range of dates on which experiments were conducted were chosen for sampling to evaluate the condition of the material. This limited the potential for contamination or oxidation compared with sampling all the ampules. Samples were chosen blindly on a given date. Samples were not selected randomly as this was not to characterize the whole of the material but to look for differences in results given the evolving nature of the synthesis method. This is a reference material (RM) for use and evaluation by the analytical community rather than a standard reference material (SRM). The focus during the inspection of the ampules was on searching for gross problems from production that would require eliminating whole ampules before mixing all synthesized pyrrhotite together to form the reference material component. If one or more samples had noteworthy differences in composition, all the ampules would have been tested. However, as described below, impurities were rare, and the pyrrhotite iron to sulfur ratios were consistent across sampled ampules.

Fig. 11 Ampules before opening.

3.1. Ampule Opening

Ampules were opened following the procedure outlined in section 2.7, ground using a ring-and-puck system to pass through a 63 µm sieve and stored under a vacuum when not used for preparation or analysis. It was observed that a minority of vessels had a notable ‘pop’ when opened, resulting in more extensive shattering of the glass ampule. This was not

expected as the partial pressure of sulfur in equilibrium with pyrrhotite is less than atmospheric pressure, and only a tiny sound of air being drawn in was expected. In the initial trials, no pop was noted. It was speculated that there remained a slight excess of vapor pressure at a temperature causing the popping sound. However, that vapor pressure also should have been less than ambient at room temperature. It is also possible that the quartz-glass tube had undergone strain in response to the stress induced by the experiment's temperature-pressure path, which was released energetically on opening.

3.2. Individual Ampule Spot Checks

3.2.1. SEM Imaging- Ampule Checks

A small portion of each sample was mounted in Epo-Fix epoxy for analysis by SEM/EDS. The contrast and brightness of the detected background were adjusted so that known control samples of hematite, pyrite, and pyrrhotite were visually distinguishable. BSE (Backscatter Electron) images were examined to evaluate the physical presentation of the sample [Fig. 12]. Grains were a mix of solid crystals that polished to a uniform flat surface and sub-grain conglomerations. In these images, the epoxy appears black. Pyrite and iron oxides such as magnetite and hematite would have appeared darker than these grains.

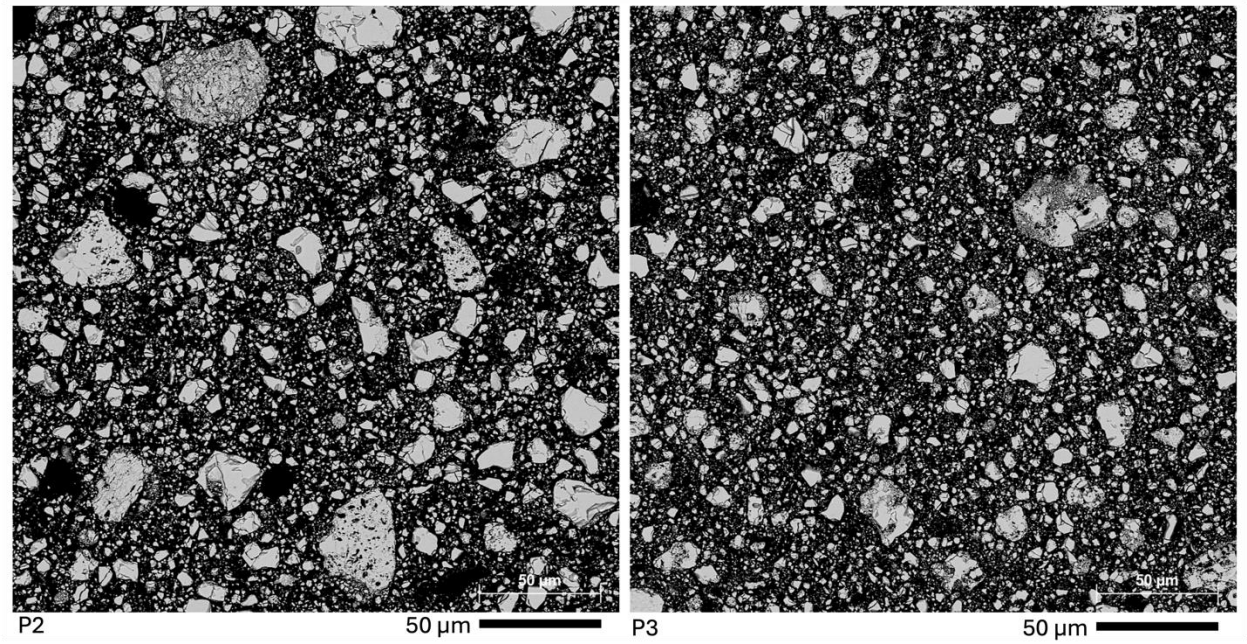

Fig. 12 SEM images of ground pyrrhotite from select ampules. Backscatter Electron (BSE) photomicrographs of pyrrhotite grains (grey) embedded in epoxy resin (black) and polished.

3.2.2. SEM Particle Analysis-Ampule Checks

Given the apparent uniformity and small particle size, an automated particle analysis that included elemental analysis by EDS was performed on a 250 µm field of view (FOV) area to

search for non-pyrrhotite grains. Particle analysis was performed using the Bruker Esprit software 'Features' method. The backscatter image is segmented based on pixel brightness against the black epoxy background. Each identified grain is scanned with the electron beam, and an EDS spectrum is recorded for 0.2 seconds. Semi-quantitative elemental abundances in atomic percent are then compared to a list of possible minerals with user-defined attributes. Pyrrhotite and pyrite were distinguished based on the Fe:S ratio. A minimum cutoff in pixels (4 pixels, 1 µm) and particle width (2 µm) was enforced to prevent the analytical volume potentially extending beyond the particle and including the epoxy. Therefore, minimum and average particle sizes listed in Table 1 are of included particles, not of *all* particles. Overall, few pyrite grains were encountered. Very few potential iron oxides were identified but could not be well distinguished from oxygen potentially coming from the epoxy and are omitted here.

Table 1 Descriptive particle characteristics.

	Pyrrhotite		Pyrite		Pyrrhotite Particle Dimensions					
Sample ID	Count n	Total Area µm^2	Count n	Total Area µm^2	Length (µm) Min	Length (µm) Max	Length (µm) Min	Length (µm) Max	Avg Diameter (µm) Avg	Avg Diameter (µm) 1σ
1	432	15997	1	9.9	3.7	52.8	3	39	6.7	4.6
2	789	20227	1	7.8	2.7	53.4	2	35.5	5.3	4
3	793	17060	2	47.4	47.4	41.8	2	33.1	5.2	3.1
4	805	17039	3	51.8	51.8	42.2	2	30.7	4.9	3.6
5	917	16971	1	4.8	4.8	50.6	2	26.4	4.9	3.1
6	661	15808	4	31.5	31.5	28.5	2.5	5.2	5.2	3.7

3.2.3. SEM/EDS Individual Grain Compositions- Ampule Checks

A spot-check of grains from each sample was performed to compare the Fe:S molar ratio of the sample to evaluate if they were pyrite (Fe:S ratio of 0.5) or pyrrhotite (Fe:S ratio of 0.88 to 0.92 depending on the polytype). Individual spectra were recorded on 10 grains in each sample for standards-based analysis using NIST DTSA II [99]. To provide adequate spectra, grains were required to be at least 5 µm in minimum diameter and have a flat polished surface. Samples were analyzed at 12 kV accelerating voltage, 3 nA beam current, for 30 seconds of live time. Spectra from two Bruker X-Flash 7 SDD EDS detectors were summed with a total detector area of 120 mm^2. Spectra were recorded from pyrite, which serves as a reference material and is mounted in the same epoxy mount and, therefore, with the same carbon coat thickness. The results are listed in Table 2 as normalized atomic percentages. The difference between ampules is less than the uncertainty within an ampule.

Table 2 SEM/EDS analyses of pyrrhotite from sampled ampules. The difference in composition among ampules is less than the standard deviation among grains within an ampule.

	Iron (atom %)	1σ	Sulfur (atom %)	1σ	Fe:S Ratio
1	47.20	0.06	52.80	0.06	0.89
2	47.15	0.11	52.85	0.11	0.89
3	47.12	0.09	52.88	0.09	0.89
4	47.14	0.11	52.86	0.11	0.89
5	47.18	0.12	52.82	0.12	0.89
6	47.13	0.12	52.87	0.12	0.89

3.2.4. XRD Analysis-Ampule Checks

The six opened ampules were analyzed by XRD to inspect for large fractions of unwanted phases (e.g., pyrite, hematite, magnetite, quartz) and to look for gross differences between the samples prepared using methods refined during the project [Fig. 13]. Samples were analyzed with a Malvern Panalytical Empyrean diffractometer using a Cu K α X-ray tube at 45 kV, scan range 12 degrees to 110 degrees, step size 0.0263 degrees, PHD lower level 45 and upper level 80, and collection time of 16 minutes. The spectra do not show notable differences among the samples. Peaks were consistent with pyrrhotite locations and other phases were not noted. Section 3.3.2 provides a more comprehensive XRD analysis of the reference material.

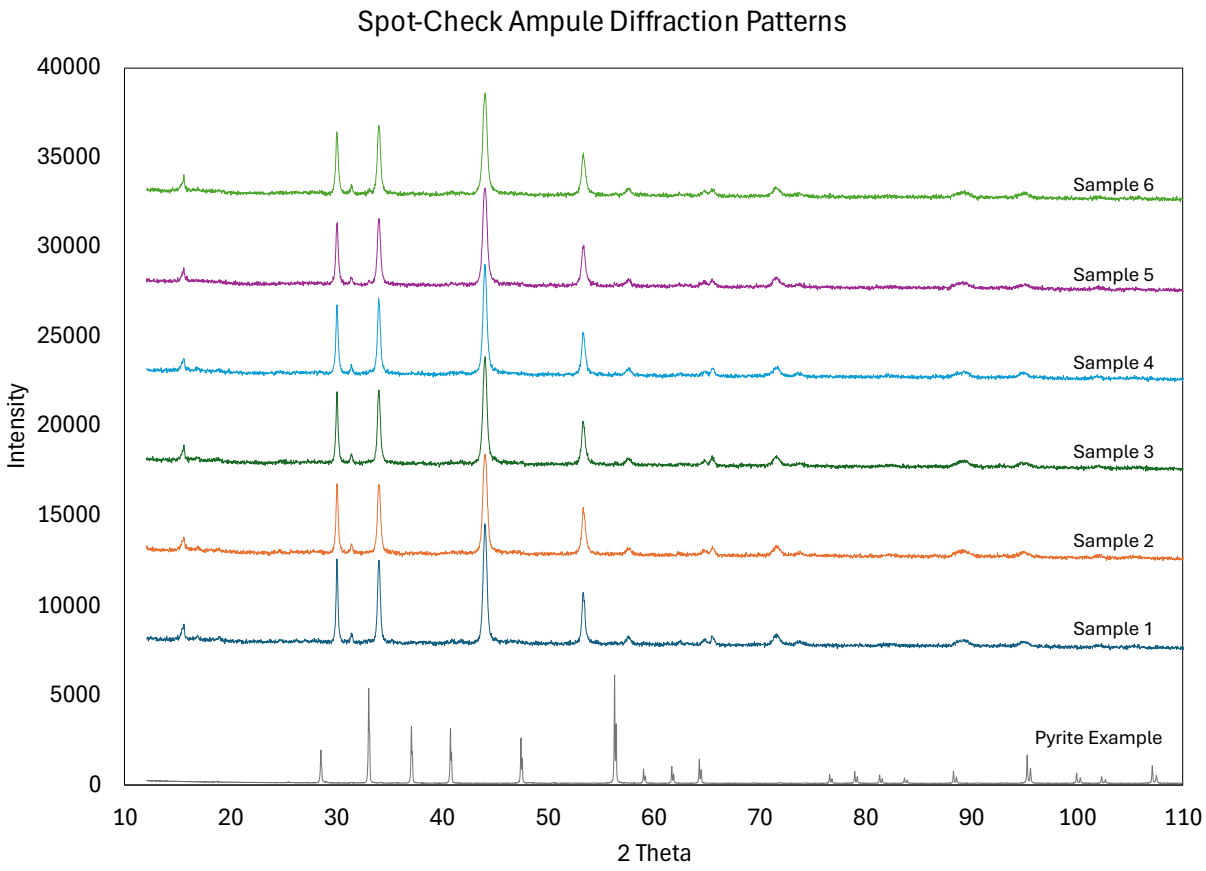

Fig. 13 X-Ray diffraction patterns from ampules chosen for sampling. Patterns are offset for clarity. No large differences were observed between samples. Oxides and pyrite were not observed.

3.3. Spot Checks of Mixed and Bottled Reference Material

Samples were bottled under nitrogen gas and sealed in evacuated packaging at NIST Office of Reference Materials. A total of 254 samples of the reference material pyrrhotite were made and numbered. Five samples were randomly selected and opened for analysis by XRD and SEM to evaluate whether the material had oxidized during handling, contamination by foreign materials had occurred, or if the composition varied greatly among samples due to the bottling process.

3.3.1. SEM Analysis

Samples from each of the five vials chosen for analysis were mounted in epoxy and polished to a 0.25 µm finish for analysis by SEM and EDS. One hundred grains in each sample were selected at random and analyzed. The beam voltage was 15 kV, and the current was 5 nA. A FOV of 1 µm was used for measurement. A difference in iron content of 0.7 atomic % separates Fe_7S_8 and Fe_9S_{10}. Counting statistics for the measurements

indicates an uncertainty of 0.1 % (one standard deviation, 1σ) for iron (which has the greater uncertainty), allowing the distinction to be made between these phases. Prior to analysis, spectra were collected from a pyrrhotite reference material (Microanalysis Consultants Ltd., UK) of composition Fe_7S_8 and were used to standardize the sample analyses using Bruker Esprit software and ϕρz (phi-rho-Z) quantitative correction method. Standards-based EDS can be used on geologic materials to improve the reliability of measurements and in cases with overlapping peaks [100]. Spectra were also recorded on a pyrite reference material (Microanalysis Consultants Ltd., UK) and a sample of pyrite (Wards Scientific) included in the sample mount along with the pyrrhotite and therefore having undergone the same polishing and carbon coating procedure. A sample of troilite (FeS) was measured before and after the pyrrhotite samples to look for any deviation over the time of the analyses. The grains to be analyzed were chosen to be flat, well-polished, and at least 3 µm in minimum diameter. The standard deviation of five points was less than 0.1 % for each [Table 3] reference analyzed as an unknown. All five samples were within the uncertainty of the expected value for Fe_7S_8 and within the uncertainty of each other. Sample spectra were additionally processed using NIST DTSA [99] software using the XPP Simplified ϕρz quantitative algorithm and values were similarly within uncertainty.

Table 3 SEM/EDS analyses of pyrrhotite from sampled RM vials. Sample averages are within uncertainty of expected values and each other.

		Normalized Atomic %				Weight %					
Sample ID	**n**	**Sulfur**	1σ	**Iron**	1σ	**Sulfur**	1σ	**Iron**	1σ	**Sum**	1σ
315	**100**	**53.4**	*0.1*	**46.6**	*0.1*	**39.5**	*0.2*	**60.2**	*0.3*	**99.7**	*0.4*
291	**100**	**53.4**	*0.2*	**46.6**	*0.2*	**39.6**	*0.2*	**60.2**	*0.3*	**99.8**	*0.3*
143	**100**	**53.4**	*0.2*	**46.6**	*0.2*	**39.7**	*0.2*	**60.3**	*0.4*	**100.0**	*0.5*
56	**100**	**53.3**	*0.2*	**46.7**	*0.2*	**39.6**	*0.2*	**60.4**	*0.4*	**100.0**	*0.4*
32	**100**	**53.3**	*0.1*	**46.7**	*0.1*	**39.4**	*0.2*	**60.1**	*0.2*	**99.6**	*0.4*
Pyrite std	**5**	**66.66**	*0.05*	**33.34**	*0.05*	**53.4**	*0.1*	**46.5**	*0.1*	**100.0**	*0.2*
Pyrite mounted	**5**	**66.68**	*0.06*	**33.32**	*0.06*	**53.5**	*0.1*	**46.6**	*0.1*	**100.1**	*0.2*
Troilite std start	**5**	**49.95**	*0.05*	**50.05**	*0.05*	**36.5**	*0.1*	**63.7**	*0.3*	**100.2**	*0.4*
Troilite std end	**5**	**50.00**	*0.05*	**50.00**	*0.05*	**36.3**	*0.2*	**63.2**	*0.2*	**99.4**	*0.3*
Reference values											
Fe_7S_8 (4C)		**53.3**		**46.7**		**39.6**		**60.4**		**100.0**	
Fe_9S_{10} (5C/7C)		**52.6**		**47.4**		**38.9**		**61.1**		**100.0**	
$Fe_{10}S_{11}$ (11C)		**52.4**		**47.6**		**38.7**		**61.3**		**100.0**	
$Fe_{11}S_{12}$ (6C)		**52.2**		**47.8**		**38.5**		**61.5**		**100.0**	

Tescan Mira 4 FE-SEM, two Bruker Xflash 7 EDS detectors (120 mm^2 total collector area), 15 kV, 5.0 nA, 5 second collection time, 1 µm FOV spot size, standardized on Fe_7S_8.

3.3.2. XRD Analysis

In contrast to the SEM analysis, where only a minute amount is sampled, the XRD analysis examined approximately 4 grams of the 5-gram bottles. This analysis was performed as in section 3.2.4, except that a higher PHD (pulse height distribution) setting was used better to screen out the fluorescence from iron in the sample, and a smaller step size was used to attempt to differentiate among pyrrhotite polytypes. Samples were analyzed with a Malvern Panalytical Empyrean diffractometer using a Cu K α X-ray tube at 45 kV, scan range 12 degrees to 110 degrees, step size 0.0131, PHD lower level 52 and upper level 70, and a collection time of 70 minutes. X-ray diffraction patterns from the five samples are shown in Fig. 14 X-Ray diffraction patterns from sample reference material vials. Patterns are offset for clarity. Samples all index as Monoclinic. Larger pyrrhotite peaks are labeled (hkl). Small peaks from pyrite are labeled (py). Patterns are consistent across samples. Example simulated patterns are shown in the inset to illustrate the small differences between them. The RM likely contains some high-temperature 3C as well as 5C polytypes of pyrrhotite and < 1 weight % of pyrite based on XRD fitting of patterns. The five samples are offset for clarity. The diffraction patterns all index as Monoclinic. The major peaks are identified in the plot. Some small peaks align with the most substantial peaks of pyrite, indicated by the abbreviation “py.” Rietveld refinement gave an estimate for pyrite < 1 wt. % which is less than the quantitation limit for this technique, but some is known to be present based on SEM examination of the RM. No iron oxide patterns were matched. Simulated diffraction scans (inset box) of five pyrrhotite polytypes are included for reference. Rietveld refinement suggests that most of the pyrrhotite is the 4C type, but some amount of the high-temperature form of Fe_7S_8 is present along with some amount of the 5C Fe_9S_{10} type. The similarity of the patterns makes this distinction very difficult, and in an analysis against other mineral phases, the RM should match as pyrrhotite without difficulty. A sample of the RM was also mixed with Al_2O_3 (30 weight %) for use as an internal standard. The amorphous content was calculated to be < 0.2 %, well below the limit of quantification, and there is no reason to suspect the RM pyrrhotite is not fully crystalline.

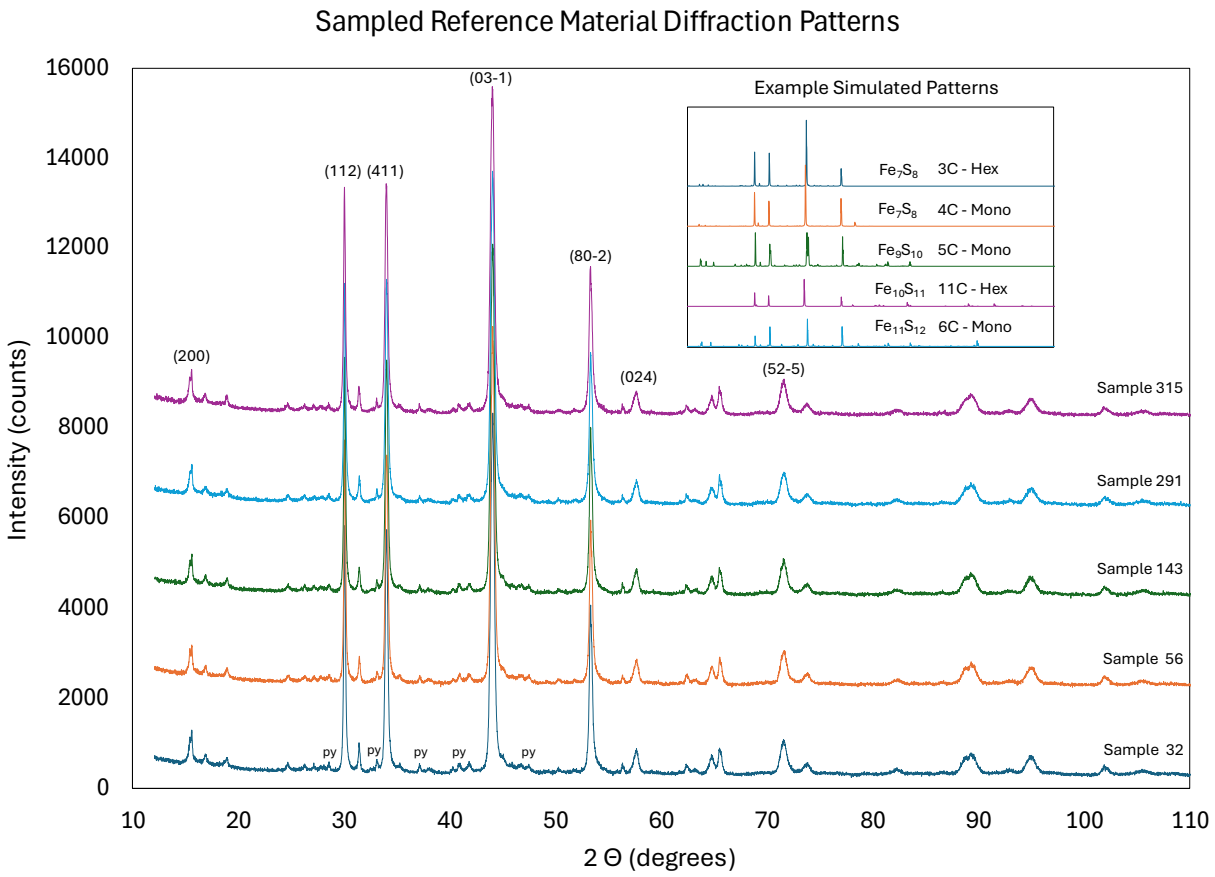

Fig. 14 X-Ray diffraction patterns from sample reference material vials. Patterns are offset for clarity. Samples all index as Monoclinic. Larger pyrrhotite peaks are labeled (hkl). Small peaks from pyrite are labeled (py). Patterns are consistent across samples. Example simulated patterns are shown in the inset to illustrate the small differences between them. The RM likely contains some high-temperature 3C as well as 5C polytypes of pyrrhotite and < 1 weight % of pyrite based on XRD fitting of patterns.

4. Conclusions

In response to the ongoing challenges presented by the inclusion of pyrrhotite-containing aggregate in residential foundations, NIST has prepared a reference material (RM 8154) to aid in the development of techniques to determine the presence and concentration of sulfur due to pyrrhotite in aggregate and concrete materials. Iron and sulfur reagents were reacted following a specific temperature profile within sealed evacuated quartz-glass ampules. The development of this technique from the scale of a few grams to 1.8 kg required careful consideration of the safety and efficacy of the design and methods used. Two hundred fifty-four samples containing 5 grams of synthesized pyrrhotite of predominantly monoclinic Fe_7S_8 composition were produced. Spot checks of the final product did not reveal problems that would prevent its use in the reference material. The community will evaluate the ultimate composition of the reference material components in an interlaboratory study.

5. References

[1] United States Government Accountability Office (2020) Crumbling Foundations: Extent of Homes with Defective Concrete Is Not Fully Known and Federal Options to Aid Homeowners Are Limited.

[2] Federal Emergency Management Agency (2018) Connecticut's Crumbling Concrete: Coordinating Federal Resources for a Non-Stafford Act Event.

[3] Jana D (2022) Cracking of residential concrete foundations in eastern Connecticut, USA from oxidation of pyrrhotite. *Case Studies in Construction Materials* 16. https://doi.org/10.1016/j.cscm.2022.e00909

[4] Zhong R, Wille K (2018) Deterioration of residential concrete foundations: The role of pyrrhotite-bearing aggregate. *Cement and Concrete Composites* 94. https://doi.org/10.1016/j.cemconcomp.2018.08.012

[5] Tagnit-Hamou A, Saric-Coric M, Rivard P (2005) Internal deterioration of concrete by the oxidation of pyrrhotitic aggregates. *Cement and Concrete Research* 35(1). https://doi.org/10.1016/j.cemconres.2004.06.030

[6] Jana D (2024) Preventing Pyrrhotite Damage in Concrete Proposal for a performance-based testing protocol. *Concrete International* 46:42–47. Available at www.concreteinternational.com

[7] Bentivegna AF, Snyder A, Stacey SM (2023) Pyrrhotite in Concrete Aggregates Is legislation ahead of science? *Concrete International* 45:37–44. Available at www.concreteinternational.com|

[8] State of Connecticut Department of Consumer Protection (2016) Report on Deteriorating Concrete in Residential Foundations. (Hartford, CT).

[9] Connecticut Foundation Solutions Indemnity Company Inc (2024) President's Message. *Available at https://crumblingfoundations.org/presidents-message/*.

[10] State of Connecticut (2021) *An Act Concerning Crumbling Concrete Foundations* (https://www.cga.ct.gov/2021/act/Pa/pdf/2021PA-00120-R00HB-06646-PA.PDF), Substitute House Bill No. 6646, Public Act No. 21-120.

[11] Commonwealth of Massachusetts (2021) *An Act Relative to Crumbling Concrete Foundations* (https://malegislature.gov/Bills/192/S548), Senate Bill No. 548.

[12] Arndt N, Kesler S, Ganino C (2015) *Metals and society: An introduction to economic geology, second edition*. https://doi.org/10.1007/978-3-319-17232-3

[13] Toulmin P, Barton PB (1964) A thermodynamic study of pyrite and pyrrhotite. *Geochimica et Cosmochimica Acta* 28(5). https://doi.org/10.1016/0016-7037(64)90083-3

[14] Fleet ME (2006) *Phase equilibria at high temperatures*, Vol. 61. https://doi.org/10.2138/rmg.2006.61.7

[15] Arnold RG (1967) Range in composition and structure of 82 natural terrestrial pyrrhotites. *The Canadian Mineralogist*.

[16] Byström A (1945) Monoclinic magnetic pyrites. *Mineralogi och Geologi* 19B(8):1–8.

[17] Bertaut EF (1952) La structure de la pyrrhotine Fe7S8", . *Comptes rendus des śéances de l'Academie des Sciences* 234:1295–1297.

[18] Grønvold F, Haraldsen H, Faurholt C (1952) On the Phase Relations of Synthetic and Natural Pyrrhotites (Fe(1-x)S). *Acta Chemica Scandinavica* 6. https://doi.org/10.3891/acta.chem.scand.06-1452

[19] Von Gehlen (1963) Phase relations at low temperatures. *Carnegie Institute of Washington* Yearbook 63.

[20] Kullerud G (1967) Sulfide Studies. *Researches in Geochemistry*, ed Ablesone PH (John Wiley and Sons, Inc., New York), Vol. 2, pp 286–321.

[21] Taylor LA (1970) Low-temperature phase relations in the Fe-S system. *Carnegie Institute of Washington, Yearbook 68*:259–270.

[22] O'Reilly W, Hoffmann V, Chouker AC, Soffel HC, Menyeh A (2000) Magnetic properties of synthetic analogues of pyrrhotite ore in the grain size range 1-24 μm. *Geophysical Journal International* 142(3). https://doi.org/10.1046/j.1365-246X.2000.00169.x

[23] Mengason MJ, Piccoli PM, Candela P (2010) An evaluation of the effect of copper on the estimation of sulfur fugacity (fS2) from pyrrhotite composition. *Economic Geology* 105(6). https://doi.org/10.2113/econgeo.105.6.1163

[24] Powell A V., Vaqueiro P, Knight KS, Chapon LC, Sánchez RD (2004) Structure and magnetism in synthetic pyrrhotite Fe7S 8: A powder neutron-diffraction study. *Physical Review B - Condensed Matter and Materials Physics* 70(1). https://doi.org/10.1103/PhysRevB.70.014415

[25] Belzile N, Chen YW, Cai MF, Li Y (2004) A review on pyrrhotite oxidation. *Journal of Geochemical Exploration* 84(2). https://doi.org/10.1016/j.gexplo.2004.03.003

[26] Belzile N, Maki S, Chen YW, Goldsack D (1997) Inhibition of pyrite oxidation by surface treatment. *Science of the Total Environment* 196(2). https://doi.org/10.1016/S0048-9697(96)05410-1

[27] Johnson RH, Blowes DW, Robertson WD, Jambor JL (2000) The hydrogeochemistry of the Nickel Rim mine tailings impoundment, Sudbury, Ontario. *Journal of Contaminant Hydrology* 41(1–2). https://doi.org/10.1016/S0169-7722(99)00068-6

[28] Haugen H, Lindgård J (2018) Determination of Total Sulphur Content in Aggregates (2004-2018) - Results From SINTEF. *Workshop Proceedings No. 14* (The Nordic Concrete Federation, Oslo, Norway).

[29] Pyy H (2018) Cases in Finland where sulphide minerals in aggregate have caused damages in Concrete structures. *Workshop Proceedings No. 14, The Nordic Concrete Federation (Oslo, Norway, 2018)* (The Nordic Concrete Federation, Oslo, Norway).

[30] Moum J, Rosenqvist ITH (1959) Sulfate Attack on Concrete in the Oslo Region. *ACI Journal Proceedings* 56(9). https://doi.org/10.14359/8095

[31] Schmidt T, Leemann A, Gallucci E, Scrivener K (2011) Physical and microstructural aspects of iron sulfide degradation in concrete. *Cement and Concrete Research* 41(3). https://doi.org/10.1016/j.cemconres.2010.11.011

[32] Ayora C, Chinchón S, Aguado A, Guirado F (1998) Corrigendum to "Weathering of iron sulfides and concrete alteration: Thermodynamic model and observation in dams from Central Pyrenees, Spain" (Cement and Concrete Research Volume 28

Issue 4 Page 591-603 Published APR1998). *Cement and Concrete Research* 28(9). https://doi.org/10.1016/s0008-8846(98)00137-9

[33] Araújo GS, Chinchón S, Aguado A (2008) Evaluation of the behaviour of concrete gravity dams suffering from internal sulfate attack. *Ibracon Structures and Materials Journal* 1:17–45.

[34] Oliveira I, Cavalaro SHP, Aguado A (2014) Evolution of Pyrrhotite Oxidation in Aggregates for Concrete. *Materiales De Construcción* 64(316).

[35] Chinchón JS, Ayora C, Aguado A, Guirado F (1995) Influence of weathering of iron sulfides contained in aggregates on concrete durability. *Cement and Concrete Research* 25(6). https://doi.org/10.1016/0008-8846(95)00119-W

[36] Chinchón-Payá S, Aguado A, Chinchón S (2012) A comparative investigation of the degradation of pyrite and pyrrhotite under simulated laboratory conditions. *Engineering Geology* 127. https://doi.org/10.1016/j.enggeo.2011.12.003

[37] Rodrigues A, Duchesne J, Fournier B, Durand B, Rivard P, Shehata M (2012) Mineralogical and chemical assessment of concrete damaged by the oxidation of sulfide-bearing aggregates: Importance of thaumasite formation on reaction mechanisms. *Cement and Concrete Research* 42(10). https://doi.org/10.1016/j.cemconres.2012.06.008

[38] Duchesne J, Fournier B (2013) Deterioration of Concrete by the Oxidation of Sulphide Minerals in the Aggregate. *Journal of Civil Engineering and Architecture* 7(69).

[39] McCarthy D, Kane N, Lee F, Blaney D (2017) Report of the Expert Panel on Concrete Blocks. (Dublin). Available at https://www.gov.ie/en/publication/0218f-report-of-the-expert-panel-on-concrete-blocks/

[40] Leemann A, Lothenbach B, Münch B, Campbell T, Dunlop P (2023) The “mica crisis” in Donegal, Ireland – A case of internal sulfate attack? *Cement and Concrete Research* 168. https://doi.org/10.1016/j.cemconres.2023.107149

[41] Brough C, Staniforth B, Garner C, Garside R, Colville R, Strongman J, Fletcher J (2023) High risk concrete blocks from County Donegal: The geology of defective aggregate and the wider implications. *Construction and Building Materials* 408. https://doi.org/10.1016/j.conbuildmat.2023.133404

[42] Leemann A, Münch B, Lothenbach B, Winnefeld F, Dunlop P (2024) Defective homes in Donegal, Ireland: effect of exposure conditions and concrete quality on pyrrhotite oxidation and internal sulfate attack. *SSRN Electronic Journal*:1–29.

[43] Rodgers J (1985) *Bedrock Geological Map of Connecticut* (Connecticut Geological and Natural History Survey, Hartford, CT).

[44] Connecticut Geological Survey (2013) *Generalized Bedrock Map of Connecticut* (Department of Energy and Environmental Protection).

[45] AGUE JJ (1995) Deep crustal growth of quartz, kyanite and garnet into large-aperture, fluid-filled fractures, north-eastern Connecticut, USA. *Journal of Metamorphic Geology* 13(2). https://doi.org/10.1111/j.1525-1314.1995.tb00220.x

[46] Peper JD, Pease MHJR, Seiders V (1975) *Stratigraphic and Structural Relationships of the Brimfield Group in Northeast-Central Connecticut and Adjacent Massachusetts, Geological Survey Bulletin 1389* (United States Government Printing Office, Washington, DC).

[47] Snyder G (1964) *Petrochemistry and Bedrock Geology of the Fitchville Quadrangle Connecticut, Geological Survey Bullitin 1161-1 (USGS)* (United States Government Printing Office, Washington, DC).
[48] Du R, Xian H, Wu X, Zhu J, Wei J, Xing J, Tan W, He H (2021) Morphology dominated rapid oxidation of framboidal pyrite. *Geochemical Perspectives Letters* 16. https://doi.org/10.7185/GEOCHEMLET.2104
[49] Clifton JR, Pommersheim JM (1994) Sulfate attack of cementitious materials: volumetric relations and expansions. *National Institute of Standards and Technology (NIST) Internal Report 5390*.
[50] Casanova I, Agulló L, Aguado A (1996) Aggregate expansivity due to sulfide oxidation - I. Reaction system and rate model. *Cement and Concrete Research* 26(7). https://doi.org/10.1016/0008-8846(96)00085-3
[51] Zhong R, Ai X, Yao Y, Wang J, Wille K (2024) Effects of the expansion mechanisms on the pyrrhotite-induced deterioration of concrete foundations. *Case Studies in Construction Materials* 20. https://doi.org/10.1016/j.cscm.2023.e02830
[52] Divet L (2001) Internal Sulphate Reactions in Concrete. Contribution to the Study of the Mechanisms of Delayed Formation of Ettringite. (Conservatoire National des Arts et Metiers, Paris, France).
[53] Min D, Mingshu T (1994) Formation and expansion of ettringite crystals. *Cement and Concrete Research* 24(1). https://doi.org/10.1016/0008-8846(94)90092-2
[54] Diamond S (1996) Delayed ettringite formation - Processes and problems. *Cement and Concrete Composites* 18(3). https://doi.org/10.1016/0958-9465(96)00017-0
[55] Morse-Fortier LJ (2022) Concrete Damage Attributable to the Oxidation of Pyrrhotite. *Forensic Engineering 2022: Elevating Forensic Engineering - Selected Papers from the 9th Congress on Forensic Engineering*, Vol. 1. https://doi.org/10.1061/9780784484548.106
[56] Titon B, Duchesne J, Fournier B (2024) The role of biotite in the deterioration of pyrrhotite within concrete aggregates: Trois-Rivières case study. *Cement and Concrete Research* 183.
[57] Michel FM, Ehm L, Antao SM, Lee PL, Chupas PJ, Liu G, Strongin DR, Schoonen MAA, Phillips BL, Parise JB (2007) The structure of ferrihydrite, a nanocrystalline material. *Science* 316(5832). https://doi.org/10.1126/science.1142525
[58] Torres SM, Kirk CA, Lynsdale CJ, Swamy RN, Sharp JH (2004) Thaumasite-ettringite solid solutions in degraded mortars. *Cement and Concrete Research* 34(8). https://doi.org/10.1016/j.cemconres.2003.09.016
[59] Zhou Q, Byars EW, Lynsdale CJ, Cripps JC, Hill J, Sharp JH (2007) Relative resistance of Portland and Pozzolanic cements to the thaumasite form of sulfate attack (TSA). *12th International Congress on the Chemistry of Cement*.
[60] Barnett SJ, Macphee DE, Crammond NJ (2003) Extent of immiscibility in the ettringite-thaumasite system. *Cement and Concrete Composites*, Vol. 25. https://doi.org/10.1016/S0958-9465(03)00116-1
[61] Bensted J (2003) Thaumasite - Direct, woodfordite and other possible formation routes. *Cement and Concrete Composites*, Vol. 25. https://doi.org/10.1016/S0958-9465(03)00115-X

[62] Taylor HFW (1999) The Thaumasite Form of Sulfate Attack: Risks, Diagnosis, Remedial Works and Guidance on New Construction, Report of the Thaumasite Expert Group. (London).
[63] Rodrigues A, Duchesne J, Fournier B, Durand B, Shehata MH, Rivard P (2016) Evaluation protocol for concrete aggregates containing iron sulfide minerals. *ACI Materials Journal* 113(3). https://doi.org/10.14359/51688828
[64] Chinchon JS, Lopez-Soler A, Querol X, Vaquer R (1990) Determination of pyrrhotite (Fe1-xS) occurring in aggregates by X ray fluorescence. *Cement and Concrete Research* 20(3). https://doi.org/10.1016/0008-8846(90)90029-W
[65] Uhlig S, Möckel R, Pleßow A (2016) Quantitative analysis of sulphides and sulphates by WD-XRF: Capability and constraints. *X-Ray Spectrometry* 45(3):133–137. https://doi.org/10.1002/xrs.2679
[66] Chubarov V, Amosova A, Finkelshtein A (2016) X-ray fluorescence determination of sulfur chemical state in sulfide ores. *X-Ray Spectrometry* 45(6). https://doi.org/10.1002/xrs.2712
[67] Jana D (2020) Pyrrhotite epidemic in eastern Connecticut: Diagnosis and prevention. *ACI Materials Journal* 117(1). https://doi.org/10.14359/51718059
[68] Cruz-Hernandez Y, Chrysochoou M, Wille K (2020) Wavelength dispersive X-ray fluorescence method to estimate the oxidation reaction progress of sulfide minerals in concrete. *Spectrochimica Acta - Part B Atomic Spectroscopy* 172. https://doi.org/10.1016/j.sab.2020.105949
[69] Jana D (2022) Concrete deterioration from the oxidation of pyrrhotite: A state-of-the-art review. *Pyrite and Pyrrhotite: Managing the Risks in Construction Materials and New Applications* https://doi.org/10.52305/xfja6706
[70] Santos L, Wille K, Chrysochoou M (2024) Application of X-ray principles to quantify sulfur oxidation states in concrete. *Spectroscopy Letters* 57(7):377–387.
[71] Stutzman PE, Feng P, Bullard JW (2016) Phase analysis of portland cement by combined quantitative X-ray powder diffraction and scanning electron microscopy. *Journal of Research of the National Institute of Standards and Technology* 121. https://doi.org/10.6028/jres.121.004
[72] Janzen MP, Nicholson R V., Scharer JM (2000) Pyrrhotite reaction kinetics: Reaction rates for oxidation by oxygen, ferric iron, and for nonoxidative dissolution. *Geochimica et Cosmochimica Acta* 64(9). https://doi.org/10.1016/S0016-7037(99)00421-4
[73] ASTM International (2024) *ASTM C114-24 - Standard Test Methods for Chemical Analysis of Hydraulic Cement* (ASTM International, West Conshohocken, PA). https://doi.org/10.1520/C0114-24
[74] Hime WG (2001) Chemical Methods of Analysis of Concrete. *Handbook of Analytical Techniques in Concrete Science and Technology* https://doi.org/10.1016/b978-081551437-4.50006-0
[75] Marcelino AP, Calixto JM, Gumieri AG, Caldeira CL, Delbem ID, Ferreira MC (2020) A feasible evaluation protocol to determine the most reactive sulfide-bearing aggregate for use in concrete. *Construction and Building Materials* 242. https://doi.org/10.1016/j.conbuildmat.2020.118031

[76] Lorenzen L (1995) Some guidelines to the design of a diagnostic leaching experiment. *Minerals Engineering* 8(3). https://doi.org/10.1016/0892-6875(94)00122-S

[77] Guirguis B, Shehata MH (2017) A new screening test to evaluate the presence of oxidizable sulphide minerals in coarse aggregates. *Construction and Building Materials* 154. https://doi.org/10.1016/j.conbuildmat.2017.07.198

[78] Geiss CE, Gourley JR (2019) A thermomagnetic technique to quantify the risk of internal sulfur attack due to pyrrhotite. *Cement and Concrete Research* 115. https://doi.org/10.1016/j.cemconres.2018.09.010

[79] ASTM International (2019) *ASTM C295/295M-19 - Standard Guide for Petrographic Examination of Aggregates for Concrete* (ASTM International, West Conshohocken, PA). https://doi.org/10.1520/C0295_C0295M-19

[80] ASTM International (2020) *ASTM C856/C856M-20- Standard Practice for Petrographic Examination of Hardened Concrete* (ASTM International, West Conshohocken, PA). https://doi.org/10.1520/C0856_C0856M-20

[81] Poole AB, Sims I (2016) *Concrete Petrography: A Handbook of Investigative Techniques, Second Edition*. https://doi.org/10.1201/9781315181554

[82] ASTM International (2022) *ASTM C1723-16(2022)- Standard Guide for Examination of Hardened Concrete Using Scanning Electron Microscopy* (ASTM International, West Conshohocken, PA). https://doi.org/10.1520/C1723-16R22

[83] Scrivener KL (2004) Backscattered electron imaging of cementitious microstructures: Understanding and quantification. *Cement and Concrete Composites* 26(8). https://doi.org/10.1016/j.cemconcomp.2004.02.029

[84] Diamond S (2004) The microstructure of cement paste and concrete - A visual primer. *Cement and Concrete Composites* 26(8). https://doi.org/10.1016/j.cemconcomp.2004.02.028

[85] Stutzman PE (2001) Scanning Electron Microscopy in Concrete Petrography. *Materials Science of Concrete Special Volume*.

[86] Multani RS, Waters KE (2018) *A review of the physicochemical properties and flotation of pyrrhotite superstructures (4C – Fe7S8/ 5C – Fe9S10) in Ni-Cu sulphide mineral processing*, Vol. 96. https://doi.org/10.1002/cjce.23099

[87] Chinchón-Payá S, Aguado A, Coloma F, Chinchón S (2015) Study of aggregate samples with iron sulfides through micro X-ray fluorescence (μXRF) and X-ray photoelectron spectroscopy (XPS). *Materials and Structures/Materiaux et Constructions* 48(5). https://doi.org/10.1617/s11527-013-0233-z

[88] Rodrigues A, Duchesne J, Fournier B (2016) Quantitative assessment of the oxidation potential of sulfide-bearing aggregates in concrete using an oxygen consumption test. *Cement and Concrete Composites* 67:93–100. https://doi.org/10.1016/j.cemconcomp.2016.01.003

[89] Elberling B, Nicholson R V., Reardon EJ, Tibble P (1994) Evaluation of sulphide oxidation rates: a laboratory study comparing oxygen fluxes and rates of oxidation product release. *Canadian Geotechnical Journal* 31(3). https://doi.org/10.1139/t94-045

[90] Elberling B, Nicholson R V. (1996) Field determination of sulphide oxidation rates in mine tailings. *Water Resources Research* 32(6). https://doi.org/10.1029/96WR00487

[91] Rodrigues A, Duchesne J, Fournier B (2015) A new accelerated mortar bar test to assess the potential deleterious effect of sulfide-bearing aggregate in concrete. *Cement and Concrete Research* 73. https://doi.org/10.1016/j.cemconres.2015.02.012

[92] Ojo M, Kim D, Frame L, Wille K (2024) Electrochemical investigation of accelerated deterioration of concrete with iron-sulfide containing aggregates. *Cement and Concrete Research* 182:107570. https://doi.org/10.1016/j.cemconres.2024.107570

[93] Castillo Araiza R, Fournier B, Duchesne J, Rodrigues A (2023) Electrochemical activation of oxidation of sulfide-bearing aggregates in concrete specimens. *Cement and Concrete Research* 170. https://doi.org/10.1016/j.cemconres.2023.107186

[94] Vaughan DJ (2006) *Sulfide mineralogy and geochemistry: Introduction and overview*, Vol. 61. https://doi.org/10.2138/rmg.2006.61.1

[95] Kroenlein K, Muzny CD, Kazakov AF, Diky V, Chirico RD, Magee JW, Abdulagatov I, Frenkel M (2024) *NIST Standard Reference 203: TRC Web Thermo Tables (WTT) Version 2-2012-1 Professional* (National Institute of Standards and Technology, Gaithersburg, MD).

[96] Port ST, Chevrier VF (2020) Stability of pyrrhotite under experimentally simulated Venus conditions. *Planetary and Space Science* 193. https://doi.org/10.1016/j.pss.2020.105022

[97] Sugaki A, Shima H, Kitakaze A, Fukuoka M (1977) Hydrothermal synthesis of pyrrhotites and their phase relation at low temperature. *Science Reports of the Tohoku University, 3rd Series* 13(3).

[98] Tenailleau C, Etschmann B, Wang H, Pring A, Grguric BA, Studer A (2005) Thermal expansion of troilite and pyrrhotite determined by in situ cooling (873 to 373 K) neutron powder diffraction measurements . *Mineralogical Magazine* 69(2). https://doi.org/10.1180/0026461056920247

[99] RITCHIE NWM (2015) *NIST DTSA II public domain software* (National Institute of Standards and Technology), Netptune 2023-05-23.

[100] Mengason M, Ritchie N (2017) Overcoming Peak Overlaps in Titanium-and Vanadium-Bearing Materials with Multiple Linear Least Squares Fitting. *Microscopy and Microanalysis* 23(3). https://doi.org/10.1017/S1431927617000265